sustainability

MDPI

Article

CO_2 Emission and Cost Optimization of Concrete-Filled Steel Tubular (CFST) Columns Using Metaheuristic Algorithms

Celal Cakiroglu [1,*], Kamrul Islam [2], Gebrail Bekdaş [3] and Muntasir Billah [4,*]

[1] Department of Civil Engineering, Turkish-German University, İstanbul 34820, Turkey
[2] Department of Civil, Geological and Mining Engineering, Polytechnique Montréal, Montreal, QC H3C 3A7, Canada; kamrul.islam@polymtl.ca
[3] Department of Civil Engineering, İstanbul University-Cerrahpaşa, İstanbul 34320, Turkey; bekdas@istanbul.edu.tr
[4] Department of Civil Engineering, Lakehead University, Thunder Bay, ON P7B 7E1, Canada
* Correspondence: cakiroglu@tau.edu.tr (C.C.); habillah@lakeheadu.ca (M.B.)

Abstract: Concrete-filled steel tubular columns have garnered wide interest among researchers due to their favorable structural characteristics. To attain the best possible performance from concrete-filled steel tubular columns while reducing the cost, the use of optimization algorithms is indispensable. In this regard, metaheuristic algorithms are finding increasing application in structural engineering due to their high efficiency. Various equations that predict the ultimate axial load-carrying capacity (N_u) of concrete-filled steel tubular columns are available in design codes as well as in the research literature. However, most of these equations are only applicable within certain parameter ranges. To overcome this limitation, the present study adopts a recently developed set of equations for the prediction of Nu that have broader ranges of applicability. Furthermore, a newly developed metaheuristic algorithm, called the social spider algorithm, is introduced and applied in optimizing the cross-section of circular concrete-filled steel tubular columns. The improvement of the structural dimensioning under the Nu constraint is demonstrated. The objective underlying the optimization presented here is to minimize the CO_2 emission and cost associated with the fabrication of concrete-filled steel tubular stub columns. In this context, the relationships between the cross-sectional dimensioning of circular concrete-filled steel tubular columns and the associated CO_2 emissions and cost are characterized and visualized.

Keywords: concrete-filled steel tubular (CFST) columns; CO_2 emission; CO_2 minimization; cost optimization; eco-friendly design; metaheuristic algorithm; spider algorithm

Citation: Cakiroglu, C.; Islam, K.; Bekdaş, G.; Billah, M. CO_2 Emission and Cost Optimization of Concrete-Filled Steel Tubular (CFST) Columns Using Metaheuristic Algorithms. *Sustainability* **2021**, *13*, 8092. https://doi.org/10.3390/su13148092

Academic Editor: José Ignacio Alvarez

Received: 2 June 2021
Accepted: 14 July 2021
Published: 20 July 2021

1. Introduction

Increased ductility, ease of construction, and high strength are some of the advantages associated with concrete-filled steel tubular (CFST) columns. The favorable mechanical properties of these columns can be attributed to the excellent composite action between the steel tubes and the core concrete. The confinement effect on the concrete core provided by the steel tubes leads to substantially increased strength and ductility. Moreover, the concrete core has a stabilizing effect on the steel casing by delaying its inward buckling [1]. As a further benefit of this novel method, no formworks are needed during construction, and this significantly reduces the construction time and cost [2]. In addition to the benefits already mentioned, CFST columns generally exhibit higher strength, stiffness, ductility, energy dissipation, and better seismic resistance compared to reinforced concrete or steel columns [3]. In light of their many advantages over conventional technologies, CFST columns are increasing in popularity all over the world for the construction of bridges and mid-rise to high-rise buildings. A prominent use case of CFST columns, for example, was in the construction of the Taipei 101 skyscraper [4].

In recent decades, extensive experimental studies have been carried out on the structural response of CFST columns under pure compression, combined compression and

bending, and pure torsion [5–10]. The results of these studies indicate that the overall behavior of CFST columns depends on the strength of the steel and the core concrete, the geometric shape of the steel section, the thickness of the steel tubes, and the loading condition (eccentric versus concentric). Separate research programs have been dedicated to the study of slender and stub CFST columns. Uenaka et al. [11] conducted an experimental investigation of the mechanical behavior of concrete-filled double-skin tubular stub columns under axial loading, where the diameters of the inner and outer tubes and the tube wall thicknesses were the parameters governing the structural behavior. A total of 12 specimens with various diameter-to-thickness ratios were tested in this study. It was observed that all specimens failed due to local buckling of the steel tubes and shear failure of the filling concrete. Perea et al. [12] tested 18 full-scale specimens of slender CFST columns under axial loading, combined biaxial bending and axial compression, pure torsion, and combined torsion and compression. In their experiments, the tube diameters ranged between 5.56 in (14.12 cm) and 12.75 in (32.4 cm), while the column length ranged between 18 ft (5.5 m) and 26 ft (7.9 m). The results of their study showed that the equations prescribed in the AISC 360-16 code [13] are conservative in predicting the capacity of slender columns. Currently, available design standards, such as the American Institute of Steel Construction (AISC 360-16) [13], Eurocode 4 (EC4) [14], Canadian Standards Association (CSA S16-19) [15], and the Australian Steel Standard (AS 5100) [16], impose restrictions on the use of high-strength steel (HSS) and high-strength concrete (HSC) in CFST columns. In this context, relatively little experimental research has been carried out on CFST columns that use HSS and HSC [17–20]. Few recent studies have focused on the optimization of cross-sectional shapes of CFST columns and developed more accurate predictive models to estimate the capacity using various data-driven optimization and machine learning algorithms [21–24]. Although extensive research has been conducted in the last three decades on CFST columns, none of the studies have focused on minimizing the cost and CO_2 emission associated with the fabrication of CFST columns.

It is well known that a significant amount of CO_2 emission is associated with the production of concrete and steel. To provide some perspective, the production of 1 kg of concrete is associated with the emission of around 0.12 kg of CO_2 into the atmosphere, while the production of 1 kg of steel emits 1.38 kg of CO_2 [25]. (A detailed list of the CO_2 emissions corresponding to different classes of concrete is given in Table 1). According to Youn et al. [26], the conventional Portland cement industry is responsible for as much as 5% to 7% of global CO_2 emissions. Since concrete and steel are the most widely used construction materials in the world, due to their strength and durability, there is a growing effort within the construction industry to reduce their carbon footprint. Therefore, experimental studies have been carried out to find alternative cementitious materials such as alkali-activated materials with appropriate mechanical properties which could replace Portland cement [27].

Table 1. CO_2 emission of different concrete classes [27].

Concrete Class	C25	C40	C60	C80
CO_2 emission [kg/m^3]	215	272	350	394

Although the usual process of structural design prioritizes the optimization of the total structural weight or cost, in line with the commitment of the construction industry to reducing emissions, the optimization of CO_2 emissions has emerged as an important consideration in structural design. The main goal of this study is to demonstrate the feasibility of satisfying structural performance requirements of CFST columns while simultaneously achieving significant reduction in carbon emissions. In addition to carbon emission reduction, the cost of fabricating CFST columns was analyzed as an additional metric to be considered in the structural design. To this end, a novel metaheuristic optimization algorithm, called the social spider optimization, was adopted. As a measure of

the structural performance of CFST stub columns, the ultimate axial load-carrying capacity of these members was used, and the applicability of the social spider algorithm to this structural design problem was evaluated. For different levels of structural performance, cost and carbon emissions were found to be widely variable, suggesting that the adoption of effective structural optimization techniques will play a crucial role in the achievement of eco-friendly and cost-effective design.

2. CO_2 Emission and Structural Design

The literature in the field of CFST columns is mainly focused on the development of effective methods for the accurate prediction of the ultimate axial load-carrying capacity of these structural members. However, there is a gap in the literature with respect to the optimal design that minimizes CO_2 emissions and the cost of manufacturing CFST columns while satisfying structural requirements.

Yeo and Potra [28] showed that reinforced concrete frames designed in consideration of the CO_2 footprint can have 5% to 10% lower CO_2 emissions compared to a structure designed in consideration of cost but not emissions. Kayabekir et al. [29] analyzed the CO_2 emission and cost optimization of reinforced concrete cantilever retaining walls. The volume of concrete was found to have a decisive effect on the CO_2 emission and cost compared to the weight of steel used in construction. Paik and Na [30] investigated the effect on CO_2 emissions of using a voided slab system in place of an ordinary reinforced concrete slab. They observed a 15% overall reduction in CO_2 emissions as a result of using voided slabs. Although metaheuristic optimization techniques are increasingly being applied to structural optimization problems, to the best of the authors' knowledge, to date, these optimization techniques have not been applied to CFST columns.

Besides the minimization of CO_2 emissions, an effort that has gained traction in recent years, designers also endeavor to minimize the cost of production of structural members. In the present study, the unit costs of steel and concrete were used as the basis for calculations to minimize the overall structural cost. The cost of concrete per unit volume (Cc) and the cost of steel per unit weight (Cs) have been determined based on information available in the literature. Since the unit costs of steel and concrete may vary between jurisdictions, the optimization process was repeated for unit costs of concrete and steel in different jurisdictions representing two different geographic regions. Unit prices in the Czech Republic were used to represent the Central European region, while unit prices in Turkey were used to represent the Eastern Mediterranean region. The unit costs of different classes of concrete in the Czech Republic as reported by Ženíšek et al. [31], listed in Table 2 were used in this study. The unit cost of steel as reported for the same jurisdiction, 0.81 EUR/kg, was used in our calculations. For Turkey, we used the unit cost of steel as documented by the Government of Turkey [32]—3.95 Turkish Lira per kg, which converts to approximately 0.46 EUR/kg. The unit costs of concrete for this jurisdiction are also listed in Table 2.

Table 2. Unit costs of different concrete classes [31,32].

Concrete Class	C25	C40	C60
Cost/m^3 [EUR] (Czech Republic)	75.8	91.9	147.7
Cost/m^3 [EUR] (Turkey)	27.8	34.7	38.9

3. Axial Capacity of CFST Columns

Various methods have been developed to predict the load-carrying capacity (Nu) of CFST members, and these methods have been included in design codes such as ACI 318-19 [33] and AISC 360-16 [13]. However, most of these methods are only applicable when the design variables, such as the yield strength of the steel (f_y) and the compressive strength of the concrete (f'_c), are within a certain range. For example, the equations given in the AISC code can predict the ultimate load-carrying capacity (N_u) of CFST columns only for $f_y \leq 525$ MPa and for 21 MPa $\leq f'_c \leq 70$ MPa. The proper definition of the ultimate

load-carrying capacity is another crucial factor that has to be agreed upon in order to ensure a sound interpretation of the values predicted by the code equations. According to Tao et al. [34], Uy et al. [35], and Wang et al. [36], Nu is defined as the maximum load if this load level is reached while the axial strain in the steel casing is less than 0.01. Otherwise, Nu is defined as the load level that corresponds to a compressive strain of 0.01.

Sakino et al. [37] carried out a comprehensive research program for the experimental study of CFST short columns. A total of 114 specimens consisting of both hollow and concrete-filled steel tubes were tested under concentric axial load. The steel tube tensile strength in these experiments was found to vary between 400 MPa and 800 MPa, whereas the concrete compressive strength varied between 20 MPa and 80 MPa. The outside diameter of circular tubes (D) varied between 122 mm and 450 mm, whereas the wall thickness of the tubes was found to fall within the range of 2.96 mm to 9.45 mm.

The equations for the prediction of N_u developed by Wang et al. [36] consider the contributions of the steel and concrete parts of the CFST member to the axial load-carrying capacity separately, as shown in Equation (1).

$$N_u = N_s + N_c, \tag{1}$$

$$N_s = \eta_s f_y A_s,\ N_c = \eta_c f_c' A_c, \tag{2}$$

$$\eta_s = 0.95 - 12.6 f_y^{-0.85} \ln\left(\frac{0.14D}{t}\right) < 1, \tag{3}$$

$$\eta_c = 0.99 + \left[5.04 - 2.37\left(\frac{D}{t}\right)^{0.04}\left(f_c'\right)^{0.1}\right]\left(\frac{tf_y}{Df_c'}\right)^{0.51} > 1 \tag{4}$$

In Equation (1), N_s and N_c are the contributions of the steel tube and the concrete core to the ultimate strength of the member, respectively. In Equation (2), A_s and A_c are the areas of the steel tube cross-section and concrete core cross-section, respectively. Under axial load, the concrete core of the CFST column is confined by the steel tube and this confinement effect leads to the development of the hoop stresses in the steel tube which is accompanied by a decrease in the wall thickness. Therefore, the development of hoop stresses in the steel tube leads to a decrease in the axial load-carrying capacity of the steel tube. Furthermore, local buckling prior to reaching N_u can also decrease the load-carrying capacity of the steel tube. The reduction factor η_s in Equation (2) takes into account the effect of these conditions on the axial load-carrying capacity of the steel tube. In contrast to the steel tube part, the confinement by the steel tube has a favorable effect on the concrete core, and the amplification factor η_c takes into account the increase in the load-carrying capacity of the concrete core due to this confinement effect. The equations for η_s and η_c obtained through nonlinear regression are given in Equations (3) and (4). These equations are valid for CFST stub columns with a circular cross-section for certain ranges of the variables D/t, f_c', and f_y, as listed in Table 3. In Equation (3), D and t are the diameter and wall thickness of the steel tube, respectively, as depicted in Figure 1.

Table 3. Parameter ranges for which Equations (1)–(4) are applicable [36].

Diameter-to-thickness ratio	$12 \leq D/t \leq 150$
Yield strength of the steel tube	175 MPa $\leq f_y \leq$ 960 MPa
Compressive strength of the concrete	20 MPa $\leq f_c' \leq$ 120 MPa

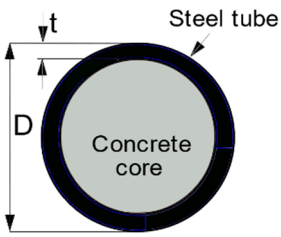

(**a**) CFST cross-section

(**b**) Shimizu Super High Rise, Japan

(**c**) Wushan Yangtze River Bridge, China

Figure 1. Diameter and wall thickness of a circular CFST column (EN 1994) and some practical application of CFST sections (adopted from Lai, 2014 [38] and Islam, 2019 [39]).

4. Metaheuristic Optimization Methodology

Metaheuristic algorithms are increasingly being applied to many challenging optimization problems. Among those algorithms, the most widespread applications in the field of engineering are the harmony search algorithm [40,41], particle swarm optimization [42], artificial bee colony technique [43,44], ant colony algorithm [45], and Jaya algorithm [46]. Alrashidi et al. [47] applied a newly developed metaheuristic algorithm, called social spider optimization (SSO), to the problem of finding the optimum probability distribution parameters to characterize the wind speeds. SSO was developed by Cuevas et al. [48]. The algorithm takes its name from a spider species called social spider that form colonies that stay together with a communal web, where the members live in close proximity to each other [49]. The communal web also acts as a medium of information transmission between the colony members. The SSO algorithm is based on the principles that govern the interactions of the social spider colony members. This technique starts with randomly generating an initial spider population of a certain size. This population consists of female and male spiders, where the males are further divided among themselves as dominant and non-dominant males. The population is divided in such a way that the females constitute 65 to 90 percent of the entire population. In this context, a spider is an abstraction for any vector of design variables that needs to be optimized. In this regard, the population is generated considering the upper and lower bounds for each one of the design variables that make up a vector of design variables. Let **S** be the set of all spiders (design vectors) and N the total number of spiders in the colony. Let $\mathbf{F} = \{f_1, f_2, \ldots, f_{Nf}\}$ and $\mathbf{M} = \{m_1, m_2, \ldots, m_{Nm}\}$ be the sets of female and male spiders, with N_f and N_m being the numbers of female and male members in the colony, respectively, such that $\mathbf{S} = \mathbf{F} \cup \mathbf{M}$ and $N = N_f + N_m$. **S** is initialized in such a way that the first N_f members of the set are females and the rest of the members are males, which results in a set $S = \{f_1, f_2, \ldots, f_{Nf}, m_1, m_2, \ldots, m_{Nm}\}$. In the current study, we are dealing with CFST column cross-sections, and each cross-section is defined by 2 design variables: the outer diameter of the circular column (D) and the wall thickness of the steel tube (t). The yield stress of steel (f_y) and the compressive strength of concrete (f'_c) are predefined constants. Each one of these parameters are kept within the boundaries given in Table 3 throughout the optimization process. Each unique combination of these parameters corresponds to a spider (design vector) in the population of spiders. The next step is to rank the population according to their fitness metric. In case of CFST column optimization, an indication of fitness could be the ultimate strength of the column, or for a fixed amount of ultimate strength, the design leading to minimum CO_2

emission or cost would be regarded as the best design (fittest spider). To this end, a weight is assigned to every design vector using Equation (5) [47].

$$w_i = \frac{F(s_i) - F(s_{worst})}{F(s_{best}) - F(s_{worst})} \quad (5)$$

In Equation (5), $F(s_i)$ represents the fitness of the i-th colony member, whereas $F(s_{best})$ and $F(s_{worst})$ represent the fitness values of the best- and worst-performing colony members, respectively.

Colony members emit vibrations to transmit various types of information through the communal web. A vibration, in particular, carries information about the relative distance and weight of a community member emitting it. Let i,j be the indices of two colony members where j is the index of the colony member emitting a vibration and i is the index of the colony member that receives that vibration. The intensity of this vibration is modeled as in Equation (6).

$$I_{i,j} = w_j \cdot e^{-d_{i,j}^2} \quad (6)$$

In Equation (6), $d_{i,j}$ is the Euclidean distance between the design vectors s_i and s_j. An issue with Equation (6) that needs to be addressed is that, for large distances, the expression for $I_{i,j}$ quickly converges to zero. In order to prevent this, all distances are scaled in such a way that the largest distance between any two members is equal to 1. There are three types of vibrations that play a role in the SSO algorithm. The first vibration type involves the case where s_j is the colony member closest to s_i with $w_j > w_i$. This type of vibration is also illustrated in Figure 2, where s3 is the closest member to s1, which also has a greater weight than s1. In the second type of vibration, s_j is the fittest member of the colony, and in the third type of vibration, s_j is the female colony member with the smallest distance from s_i. An illustration of the first vibration type is shown in Figure 2.

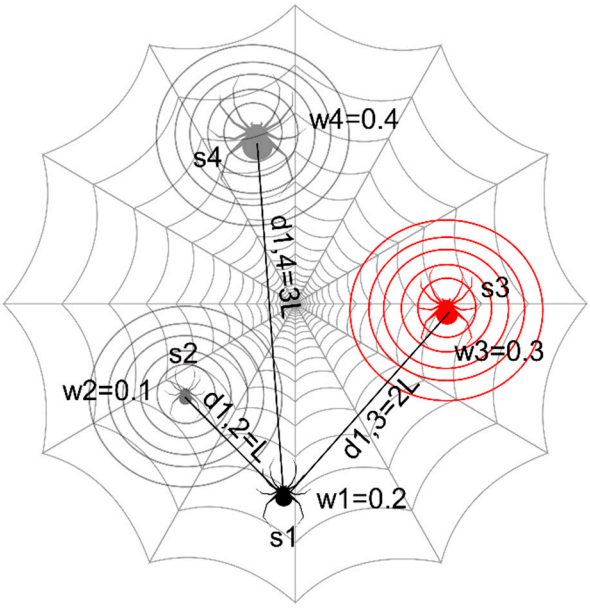

Figure 2. First type of vibration between s1 and s3.

The importance of spider gender in the SSO algorithm is that the iteration steps towards an overall better-performing community are determined by the gender. The female and male spiders exhibit different patterns of attraction and repulsion towards the other members of the colony, which determines the iteration steps of the SSO algorithm. There are three types of iteration steps called female cooperative iteration, male cooperative iteration, and mating iteration. The first and second types of vibrations have an influence

on the female iteration steps, whereas the third type of vibration plays a role in the male iteration. The female cooperative iteration formula is given in Equation (7).

$$f_i^{k+1} = \begin{cases} f_i^k + \alpha I_{i,c}\left(s_c - f_i^k\right) + \beta I_{i,b}\left(s_b - f_i^k\right) + \delta\left(\gamma - \frac{1}{2}\right) \text{ for } \varepsilon < PF \\ f_i^k - \alpha I_{i,c}\left(s_c - f_i^k\right) - \beta I_{i,b}\left(s_b - f_i^k\right) + \delta\left(\gamma - \frac{1}{2}\right) \text{ for } \varepsilon \geq PF \end{cases} \quad (7)$$

In Equation (7), $I_{i,c}$ and $I_{i,b}$ are vibration intensities perceived by f_i. $I_{i,c}$ is emitted by s_c, which is the colony member closest to f_i with a larger weight (better performance) than $f_{i,}$ and $I_{i,b}$ is emitted by s_b which is the best-performing colony member. In Equation (7), α, β, γ, δ, ε are random numbers between 0 and 1. PF is a predefined threshold value between 0 and 1 that introduces randomness (in addition to the random movement part $\delta\left(\gamma - \frac{1}{2}\right)$ into the iteration in order to better mimic the natural process of attraction or repulsion between spiders. As an example, setting PF equal to 0.7 would assign a 70% probability to the attraction of f_i towards s_c and s_b.

The iteration of a male depends on whether it is a dominant or non-dominant male. The males in a social spider population are classified as dominant and non-dominant depending on their weights (performance). To perform this classification, the males in the set **M** are sorted according to their weights from best to worst. Afterwards, all males that perform better than the median member (located in the middle of the set) are labeled as dominant, whereas the rest of the males are labeled as non-dominant. The index of this median male member in the set **S** is N_f + m. The iteration formula for males is given in Equations (8) and (9), where WMM is the weighted mean of the male population and S_f is the nearest female to m_i. The male iteration moves the dominant males towards the nearest female in the population, and the non-dominant males towards the weighted mean.

$$WMM = \frac{\sum_{h=1}^{N_m} m_h^k w_{N_f+h}}{\sum_{h=1}^{N_m} w_{N_f+h}} \quad (8)$$

$$m_i^{k+1} = \begin{cases} m_i^k + \alpha I_{i,f}\left(s_f - m_i^k\right) + \delta\left(\gamma - \frac{1}{2}\right) \text{ for } w_{N_f+i} > w_{N_f+m} \\ m_i^k + \alpha\left(WMM - m_i^k\right) \text{ for } w_{N_f+i} \leq w_{N_f+m} \end{cases} \quad (9)$$

The final step in the update of a population is the mating iteration by which potentially new members are created that replace the old members. Depending on their performance, these new members are either discarded or they replace the worst-performing members in the population. For this purpose, a new variable called the radius of mating (r) is introduced which defines an area around a dominant male such that the females within this area and the dominant male are involved in mating. The radius of mating is computed as in Equation (10), where dv_j^{high} and dv_j^{low} denote the upper and lower bounds of the j-th design variable, with n being the total number of design variables.

$$r = \frac{\sum_{j=1}^{n}\left(dv_j^{high} - dv_j^{low}\right)}{2n} \quad (10)$$

The newly generated members s_{new} have their properties assigned based on the weights of the male and females involved in the mating. In this process, those participants with greater weights also have greater influence on the properties of the new member. In case there are no females within the mating radius of a dominant male, no mating takes place in that iteration step.

Computational Procedure

The first step in this process is to generate a colony (Algorithm 1) of a certain size which is divided into females and males. This process is described with the following pseudocode where *low* and *high* are the lower and upper bounds of a particular design variable and rand $\in (0, 1)$:

Algorithm 1: Pseudocode for the initialization of the spider colony.

For *i = 1* ***to*** *N (number of colony members)*
  For *j = 1* ***to*** *n (number of design variables)*
    Spiders[i,j] = low + (high—low) (rand)
    Check if $N_u \geq N_{u,min}$
  Repeat until $N_u \geq N_{u,min}$

Since the goal of the optimization is to find the cross-section dimensions that minimize the CO_2 emission or the cost that also satisfies certain requirements for the ultimate load-carrying capacity, the random generation of design variables continues until the requirement for the ultimate load-carrying capacity is satisfied. The connectivity of the spiders inside a colony are described through the distances and perceived vibrations between any two colony members (Algorithm 2). Since the intensity of a vibration created by a colony member depends on its weight, the weights of each spider have to be computed and stored in an array. The creation of the weight array, the distance matrix, and the vibration matrix can be done as follows:

Algorithm 2: Connectivity of the spiders.

For *i = 1* ***to*** *N*
  For *j = 1* ***to*** *N*
    Distance matrix[i,j] = Distance(spiders[i], spiders[j])
    Scaled distance matrix = Distance matrix/max (Distance matrix)
For *i = 1* ***to*** *N*
  For *j = 1* ***to*** *N*
    vibration matrix[i,j] = distance(spiders[i], spiders[j])

Once the distance and vibration matrices are established, the female members of the colony (the first N_f members of the array *spiders*) make their iterative move (Algorithm 3), which is a combination of a movement towards or away from the best-performing member of the colony, the nearest better-performing member of the colony, and a random movement.

Algorithm 3: Iteration of the female spiders.

Function *move females*
Generate $\alpha, \beta, \gamma, \delta, \epsilon \in (0, 1)$
For *i = 1* ***to*** N_f
    Find the best performing and the nearest better performing members
    If $\varepsilon < 0.7$ ***then*** *apply attraction*
    Else *apply repulsion*
      Compute cross-section area and N_u
    Repeat until $N_u \geq N_{u,min}$

The next step is the movement of the dominant males towards the nearest female in the colony and the movement of the non-dominant males towards the weighted mean of the male population (Algorithm 4). To simulate this movement, first the males have to be sorted in decreasing order with respect to their weights. Afterwards, the males are divided such that all males with an index smaller than the median member are dominant and the rest of the males are non-dominant.

Algorithm 4: Iteration of the male spiders.

Function *move males*
  Compute the weighted mean of the males
  Sort the males and find the median male
  For $i = N_f$ ***to*** N
    If *Spiders[i] is dominant* ***then*** *find the nearest female to Spiders[i]*
     Apply attraction towards the nearest female
    Else *move towards the weighted mean of the male population*

After each movement, whether the updated design variables are within the allowable range or not has to be controlled (Algorithm 5).

Algorithm 5: Control of the variable ranges.

Function *control variable ranges*
  For $i = 1$ ***to*** N
  For $j = 1$ ***to*** n
    If *Spiders[i,j] violates the boundaries* ***then***
     Spiders[i] = randomly generated member
     Compute area and N_u *for the new member*
    Repeat until $N_u \geq N_{u,min}$

The last stage of the SSO iteration is the mating stage (Algorithm 6). Here, the spider with the greatest weight inside the mating set also has the highest probability of influencing the properties of the newly generated spider. A flow-chart of the entire social spider algorithm can be seen in Figure 3.

Algorithm 6: Mating.

Function *Mating*
  For $m = N_f + 1$ ***to*** N
    If *Spiders[m] is a dominant male* ***then*** *Create empty set for mating*
      For $f = 1$ ***to*** N_f
        If *Distance matrix [m,f]* $\leq$ *radius of mating*
          Add Spiders[f] to mating set
      Compute the weight distribution inside the mating set
      Generate new member with the properties of the best spider in the mating set
      If *weight of the new spider > the weight of the worst spider* ***then***
        Replace the worst spider with the new spider

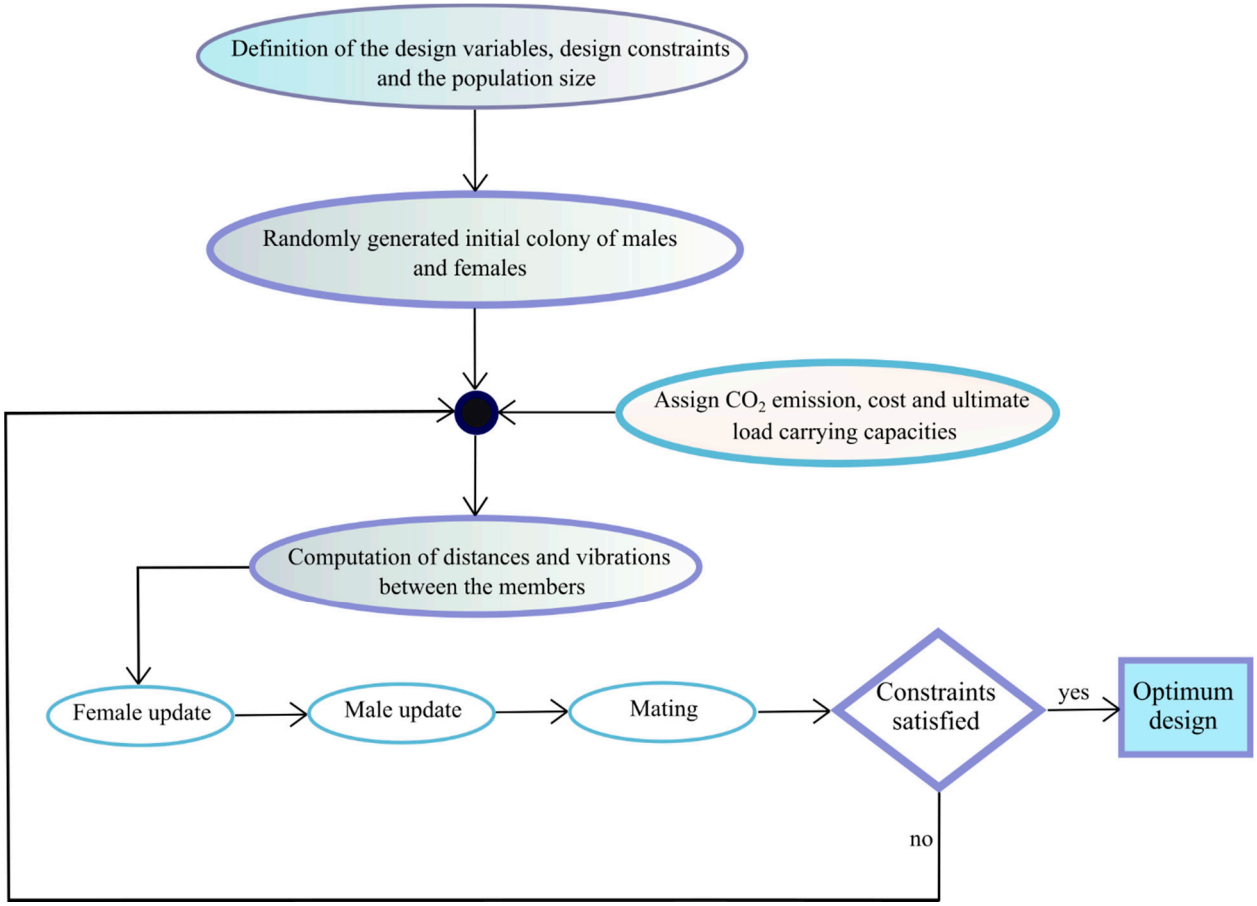

Figure 3. Flow-chart of the SSO algorithm.

5. Results and Discussions

In this section, the optimization process of the CO_2 emission and cost for circular CFST stub columns is presented for C25, C40, and C60 concrete classes. For each class, different threshold values for the ultimate axial load capacity ($N_{u,min}$) are set, and these values are used as one of the optimization constraints in addition to the dimensional constraints. For each concrete class, a value in the same order of magnitude as the ultimate axial load capacity of a specimen with the dimensions in the midrange of the values tested in the experimental study of Sakino et al. [37] was used as the threshold value for N_u. The study of Sakino et al. [37] was also used as a reference to determine upper and lower bounds for the diameter and wall thickness such that in the optimization, the outer diameter is varied in the range [122 mm, 450 mm] and the wall thickness is varied in [2.96 mm, 9.45 mm]. Using the social spider algorithm, the outer diameter and tube thickness of the member is optimized while keeping N_u above the threshold value at all times. As the optimization objectives, the CO_2 emission and cost associated with the production of a CFST column of unit height are selected.

5.1. Optimization of the CO_2 Emission

Figure 4 shows the optimization process at four different stages after 25, 50, 250, and 500 iterations. In Figure 4, the ultimate axial load-carrying capacity is kept above 6000 kN. A convergence of the minimum CO_2 emission to the vicinity of 47 kg could be observed approximately after 350 iterations, which can be confirmed by Figure 4d. An optimum diameter/thickness pair of (273.79 mm, 2.96 mm) was obtained corresponding to a CO_2 emission of 47.18 kg (Table 4) through the optimization process, using the social spider algorithm. The diameter and wall thickness values listed in Table 4 are the limit

values to which these parameters converged in the optimization process. Figure 4 shows that the most significant improvements during the optimization are observed in the first 30 iterations. After that initial phase, the optimization process continued for a total of 500 iteration steps, although only minor improvements are observed in this second phase. In the last 200 steps no further improvements could be observed, which is an indicator of convergence to an optimum (D,t) pair. In this (D,t) pair, the value of the wall thickness is equal to the lower bound for this parameter, whereas the diameter is 224% of its lower bound and 61% of its upper bound. The same procedure has been repeated for a total of six different levels of $N_{u,min}$ ranging between 6000 kN and 1000 kN, the results of which are listed in Table 4. The visualization of these results for $N_{u,min}$ = 5000 kN, 4000 kN, 2000 kN are shown in Figures 5–7, respectively.

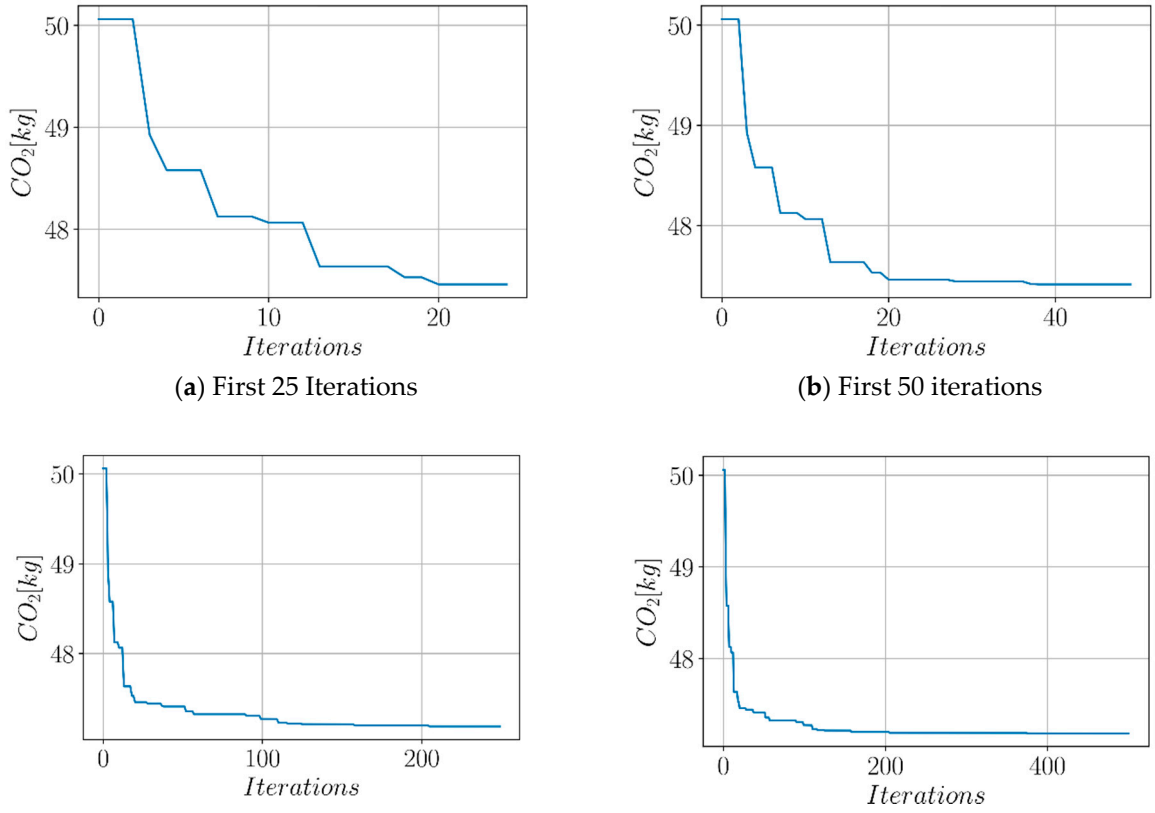

(**a**) First 25 Iterations (**b**) First 50 iterations

(**c**) First 250 iterations (**d**) First 500 iterations

Figure 4. Optimization of CO_2 emission for $N_{u,min}$ = 6000 kN. f'_c = 60 MPa.

In Figure 5, where the load capacity requirement was lowered to 5000 kN, in addition to the minimum CO_2 emission at each social spider iteration, the average CO_2 emission of the entire population has also been visualized in red color after 25, 50, 250, and 500 iterations. It can be observed that approximately 200 iterations were sufficient to bring the entire population to the optimum level for $N_{u,min}$ = 5000 kN and $N_{u,min}$ = 4000 kN. A comparison of Figures 4 and 5 reveals that lower CO_2 emission levels could be achieved in Figure 5 by decreasing the N_u requirement from 6000 kN to 5000 kN. The lowest level of CO_2 emission in 500 social spider iterations for $N_{u,min}$ = 5000 kN was 44.08 kg, which corresponds to a 6.57% reduction of CO_2 emission by a 16.7% reduction of the load-carrying capacity requirement. The optimum (diameter, wall thickness) pair for this lower load-carrying capacity requirement was (218.46 mm, 4.36 mm). A comparison to the optimum cross section for a higher load capacity shows that a lower diameter and higher wall thickness was more favorable in the optimization case with lower load capacity requirement.

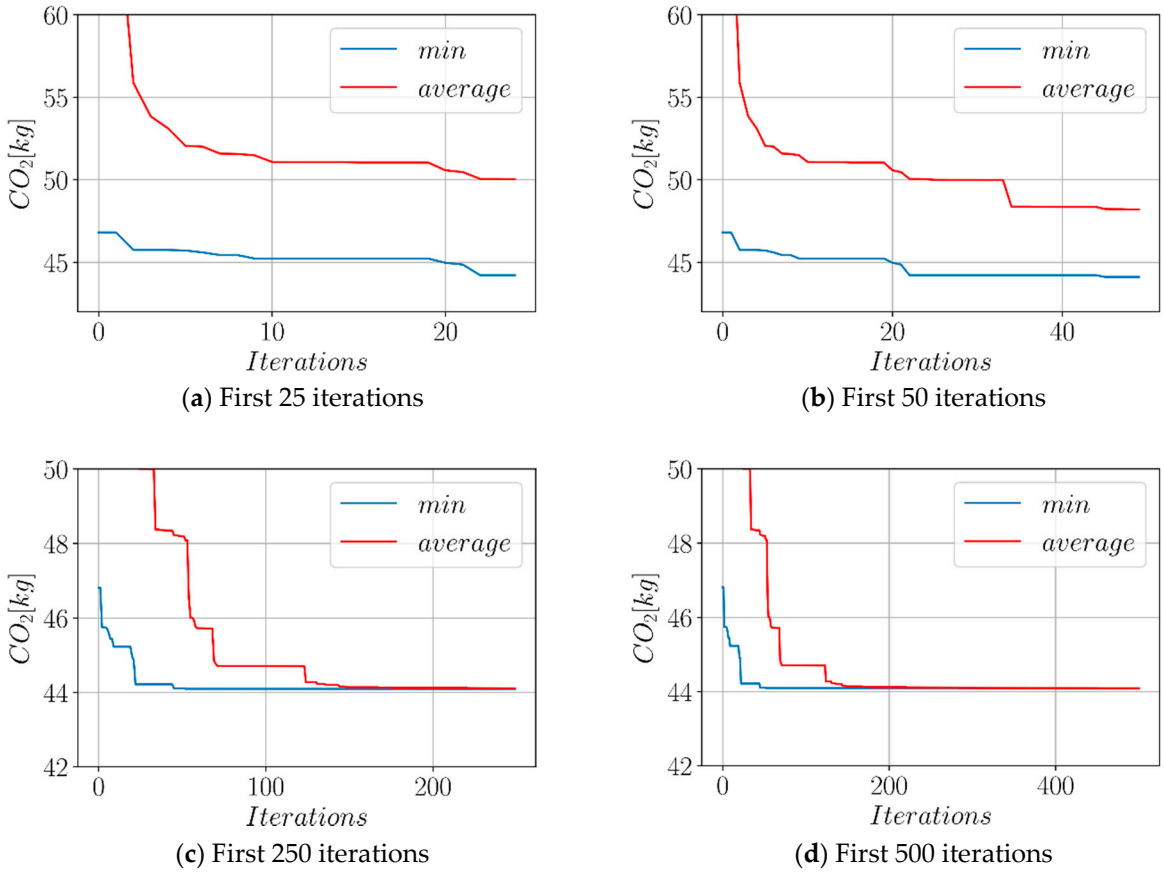

(**a**) First 25 iterations (**b**) First 50 iterations

(**c**) First 250 iterations (**d**) First 500 iterations

Figure 5. Optimization of CO_2 emission for $N_{u,min}$ = 5000 kN. f'_c = 60 MPa.

The optimization results for the reduced values of $N_{u,min}$ are visualized in Figure 6 and 7 for $N_{u,min}$ = 4000 kN and $N_{u,min}$ = 2000 kN, respectively. A more comprehensive list of the optimum combinations of diameter and wall thickness can be found in Table 4. For f'_c = 60 MPa, as the $N_{u,min}$ value decreases, the D/t ratio associated with the optimum design also decreases, except for the transition from $N_{u,min}$ = 4000 kN to $N_{u,min}$ = 3000 kN where the D/t ratio has a jump from 26.2 to 59.6. The results of the optimization process repeated for f'_c = 40 MPa and f'_c = 25 MPa are also listed in Table 4. A summary of the visualizations can also be found in Figure 8 for the first 50 social spider iterations, where the iteration steps corresponding to the different values of $N_{u,min}$ are shown with different colors.

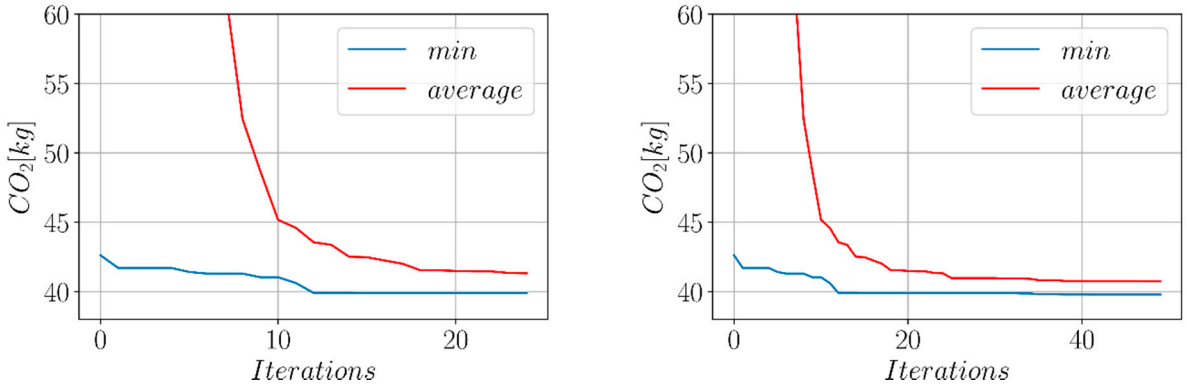

(**a**) First 25 iterations (**b**) First 50 iterations

Figure 6. *Cont.*

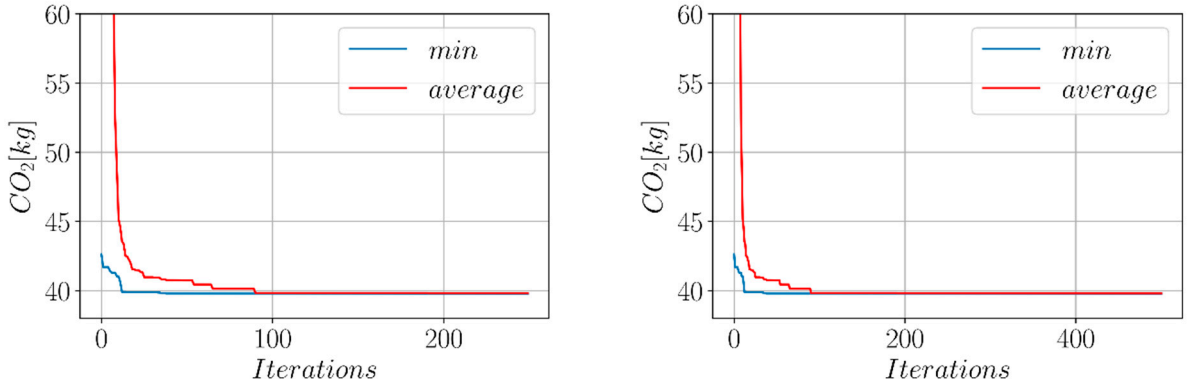

(**c**) First 250 iterations (**d**) First 500 iterations

Figure 6. Optimization of CO_2 emission for $N_{u,min}$ = 4000 kN. f'_c = 60 MPa.

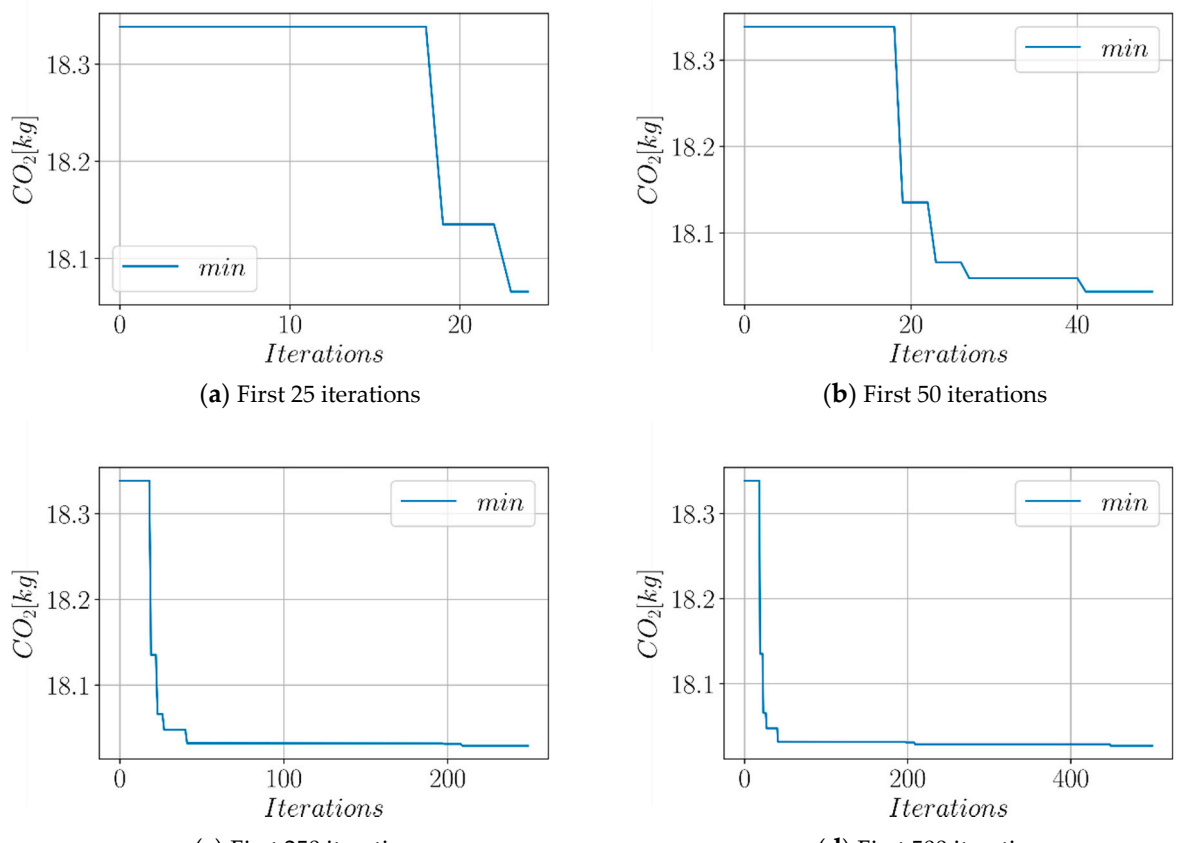

(**a**) First 25 iterations (**b**) First 50 iterations

(**c**) First 250 iterations (**d**) First 500 iterations

Figure 7. Optimization of CO_2 emission for $N_{u,min}$ = 2000 kN. f'_c = 60 MPa.

Table 4 provides a list of the cross-sectional dimensions associated with the minimum CO_2 emission for different classes of concrete and for different ultimate load-carrying capacity requirements. Within each concrete class as the load-carrying capacity requirement is lowered, the optimized cross-sections tend to have smaller outer diameters. On the other hand, the wall thicknesses show a more irregular pattern. A clear correlation can be observed between the load-carrying capacity and the CO_2 emission such that lower load-carrying capacities are associated with lower CO_2 emissions. In general, a decrease in the D/t ratio also tends to lower the CO_2 emissions except for the cases where the wall thickness significantly decreases. The wall thickness of 2.96 mm, which is the lower bound for the applicability of the equations used to calculate N_u in this work, occurs in Table 4 as the optimum wall thickness of eight configurations which indicates that smaller wall

thicknesses are more favorable in terms of CO_2 emission. Figure 9 shows the average of the six CO_2 emission values corresponding to each concrete class for C25, C40, and C60 concrete classes. From the variation of these average values, it can be inferred that using a concrete class with lower compressive strength is also conducive to lower carbon emissions.

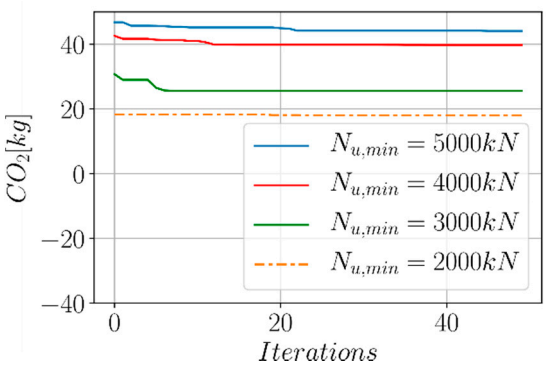

Figure 8. First 50 optimization steps for different values of $N_{u,min}$.

Table 4. Optimum configurations based on CO_2 emission.

f'_c [MPa]	D [mm]	t [mm]	D/t	$N_{u,min}$ [kN]	CO_2 [kg]
60	273.79	2.96	92.5	6000	47.18
60	218.46	4.36	50.1	5000	44.08
60	163.23	6.24	26.2	4000	39.79
60	176.47	2.96	59.6	3000	25.59
60	134.13	3.01	44.6	2000	18.03
60	122.42	3.21	38.1	1000	15.79
40	264.27	3.42	77.3	6000	44.67
40	244.52	2.96	82.6	5000	36.65
40	211.59	3.00	70.5	4000	30.46
40	176.44	2.96	59.6	3000	23.81
40	131.19	3.20	41.0	2000	17.36
40	122.55	2.98	41.1	1000	14.95
25	267.28	3.27	81.7	6000	41.03
25	244.48	2.96	82.6	5000	34.10
25	212.37	2.96	71.8	4000	28.43
25	176.47	2.96	59.6	3000	22.50
25	134.85	2.96	45.6	2000	16.20
25	124.05	8.12	15.3	1000	14.36

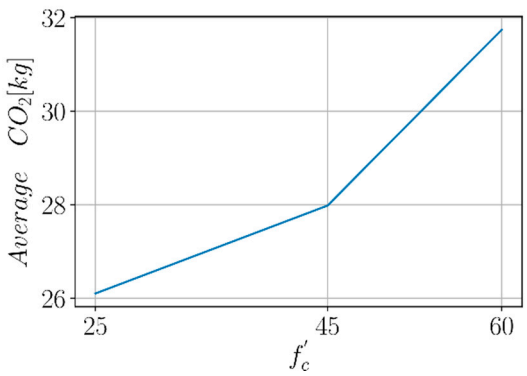

Figure 9. Average CO_2 emission for each concrete class.

For each new configuration obtained during the optimization process, there is a corresponding axial load-carrying capacity N_u which is an indicator of the structural performance. Figure 10 shows the variation of this value for the concrete classes C60 and C40. The occasional rises and falls in the value of N_u in Figure 10 indicate that, depending on the proportions of steel and concrete in the CFST column, it is possible that some configurations with smaller CO_2 emission also have better structural performance.

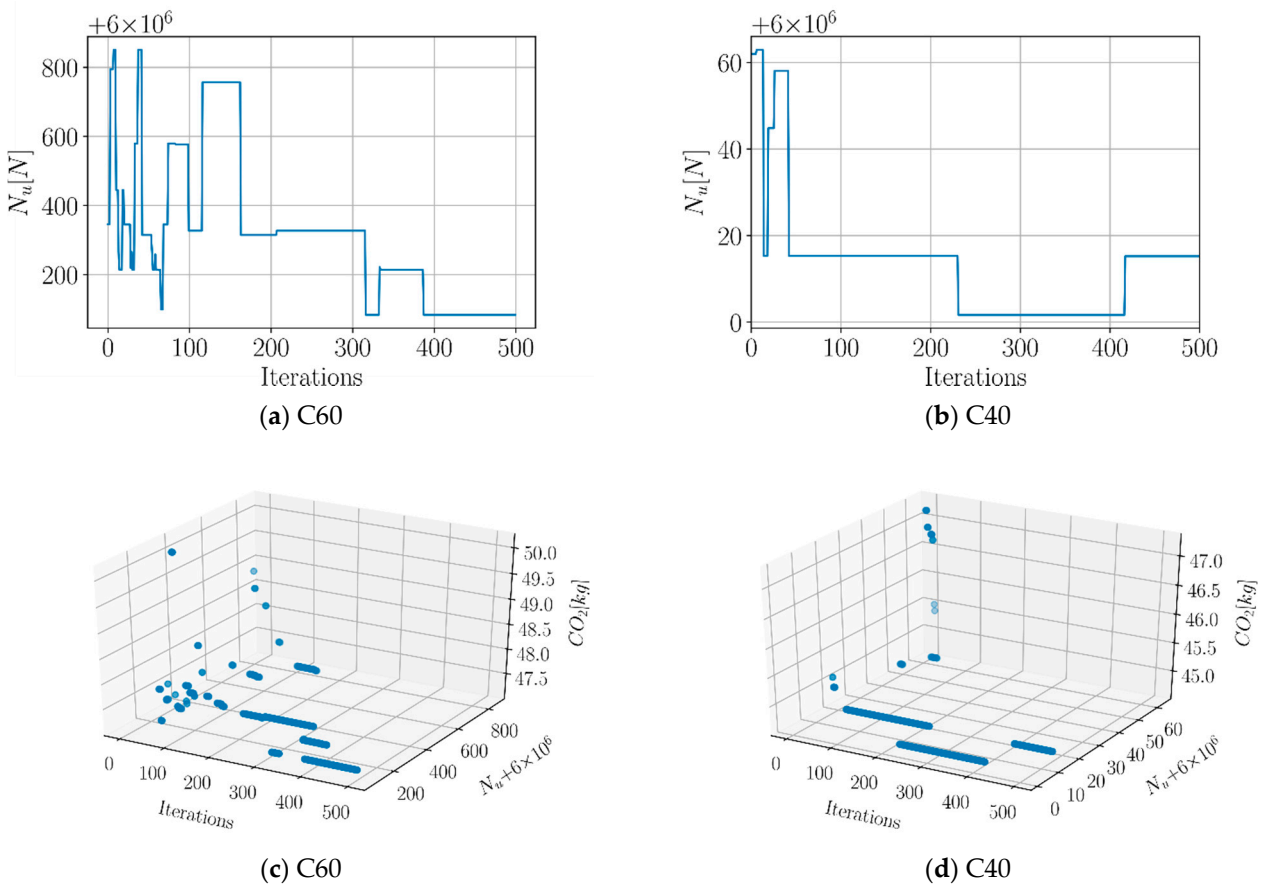

(**a**) C60 (**b**) C40

(**c**) C60 (**d**) C40

Figure 10. Variation of N_u throughout the CO_2 optimization.

5.2. Optimization of the Cost

A similar process was applied to the cost optimization as well. In order to obtain the structural dimensions that deliver the lowest cost while maintaining a certain load-carrying capacity, the social spider algorithm was applied to CFST columns with a unit height for concrete compressive strength values ranging between 25 MPa and 60 MPa and the ultimate load-carrying capacities ranging from 1000 kN to 6000 kN. Figures 11 and 12 show the minimum and average costs throughout the social spider optimization process for f'_c = 60 MPa and f'_c = 25 MPa, respectively. In each one of these figures, the optimization process is visualized at four different levels of the minimum ultimate load-carrying capacity requirement. The number of iterations included in the visualizations was adjusted so that the parts of the optimization after the convergence were mostly omitted. This procedure has been repeated considering the unit costs in two different countries (Czech Republic and Turkey). While Figures 11 and 12 depict optimization related to the unit prices in the Czech Republic, Figures 13 and 14 are based on the unit prices in Turkey. A more detailed list of the results related to cost optimization can also be found in Tables 5 and 6 for Czech Republic and Turkey prices, respectively.

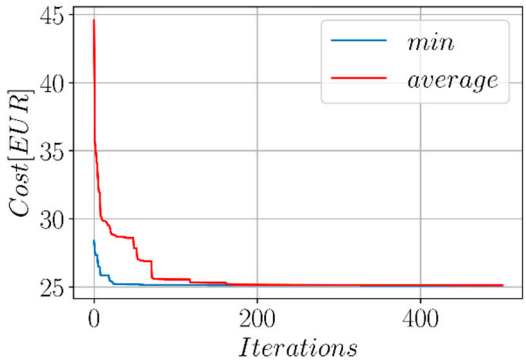

(**a**) $N_{u,min}$ = 6000 kN

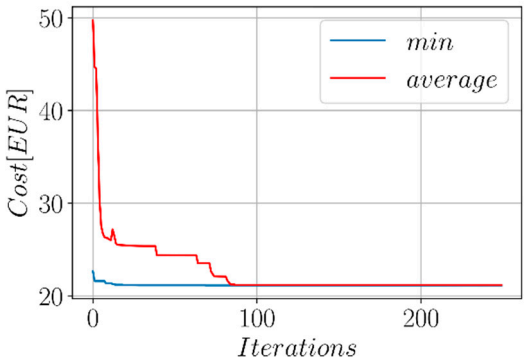

(**b**) $N_{u,min}$ = 5000 kN

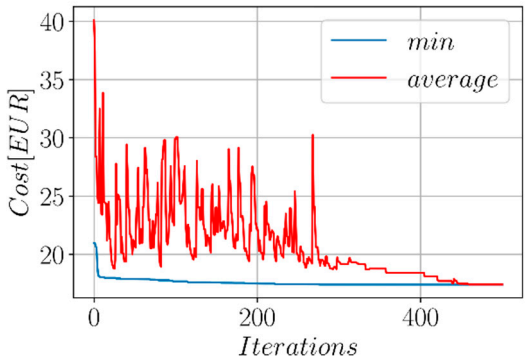

(**c**) $N_{u,min}$ = 4000 kN

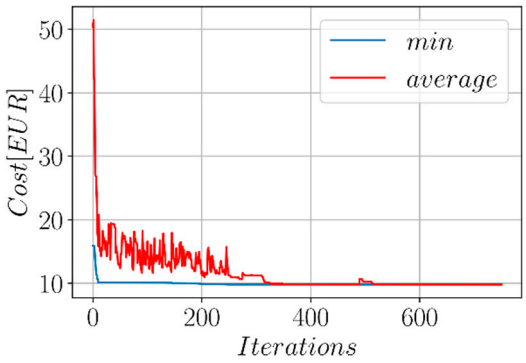

(**d**) $N_{u,min}$ = 2000 kN

Figure 11. Variation of cost for f'_c = 60 MPa, (Czech Republic).

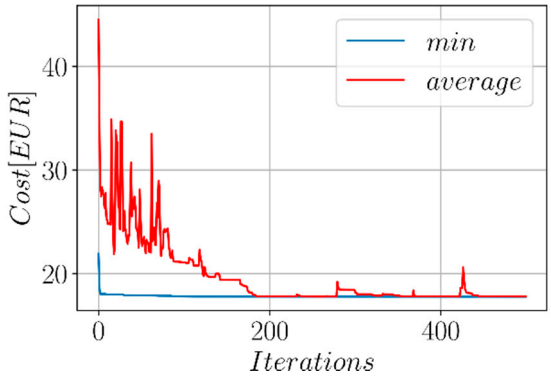

(**a**) $N_{u,min}$ = 5000 kN

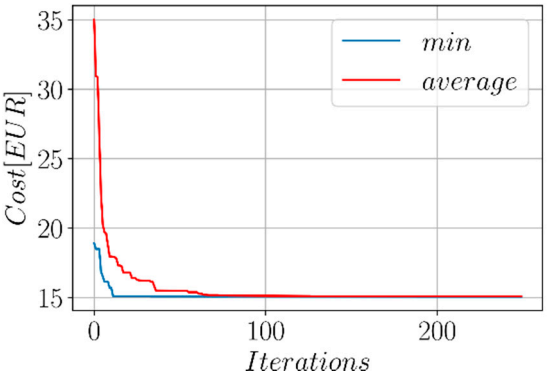

(**b**) $N_{u,min}$ = 4000 kN

Figure 12. *Cont.*

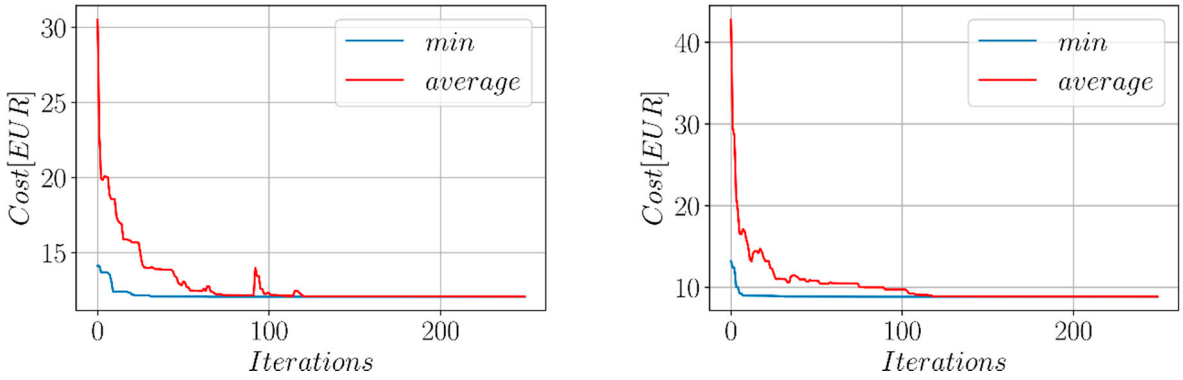

(**c**) $N_{u,min}$ = 3000 kN (**d**) $N_{u,min}$ = 2000 kN

Figure 12. Variation of cost for f'_c = 25 MPa, (Czech Republic).

From Tables 4–6 it is observed that as the $N_{u,min}$ value decreases, so does the D/t ratio in both cost and CO_2 optimization. However, there are certain differences in the speed of this decrease. In the case of CO_2 optimization, an average decrease of 30.2% is observed between two consequent $N_{u,min}$ levels. This percentage of decrease is 21.5% in the cost optimization with Czech unit prices and 16.6% in the cost optimization with Turkish unit prices. Furthermore, in cost optimization, a smaller D/t ratio was always associated with lower cost, except for one case with the lowest load-carrying capacity requirement. An observation of the values in Tables 5 and 6 shows that the concrete compressive strength and the cost associated with the production are correlated. In order to visualize this correlation, for each concrete class the average cost associated with this concrete class has been calculated and plotted in Figure 15, where the average costs in the Czech Republic and Turkey are plotted in blue and red colors, respectively. It can be seen that, as the concrete compressive strength increases, so does the average cost of producing the columns without added benefits of greater load-carrying capacity. Another inference that can be made from Tables 5 and 6 is that lowering the requirement for the load-carrying capacity results in smaller outer diameters and lower cost, whereas the wall thickness is not necessarily decreasing with the associated load-carrying capacity. Figure 16 shows the structural performance as it varies throughout the cost optimization process. Figure 17 provides an overall idea about the variation of N_u with respect to cross-sectional dimensions.

Table 5. Optimum configurations based on cost (Czech Republic).

f'_c [MPa]	D [mm]	t [mm]	D/t	$N_{u,min}$ [kN]	Cost [EUR]
60	268.32	3.22	83.33	6000	25.11
60	243.00	3.03	80.20	5000	21.14
60	212.37	2.96	71.75	4000	17.41
60	176.47	2.96	59.62	3000	13.70
60	134.90	2.96	45.57	2000	9.78
60	137.07	6.88	19.92	1000	8.66
40	273.80	2.96	92.50	6000	21.30
40	238.35	3.26	73.11	5000	19.3
40	212.49	2.96	71.79	4000	15.55
40	176.47	2.96	59.62	3000	12.43
40	134.91	2.96	45.58	2000	9.05
40	125.9	8.26	15.24	1000	8.38
25	274.02	2.96	92.57	6000	20.41
25	244.48	2.96	82.60	5000	17.76
25	211.93	2.98	71.12	4000	15.05
25	180.74	2.97	60.86	3000	12.43
25	134.90	2.96	45.57	2000	8.84
25	123.01	3.23	38.08	1000	7.90

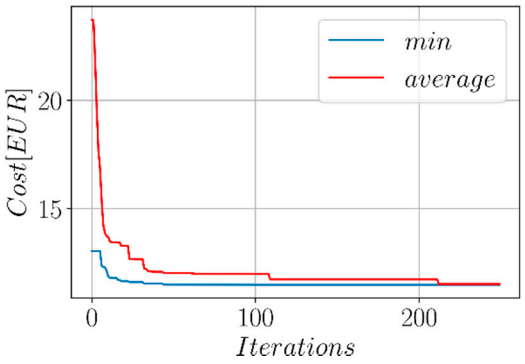

(**a**) $N_{u,min}$ = 6000 kN

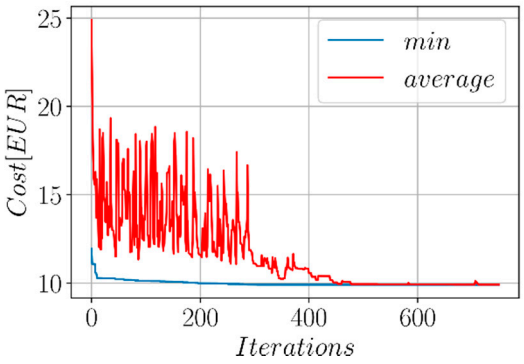

(**b**) $N_{u,min}$ = 5000 kN

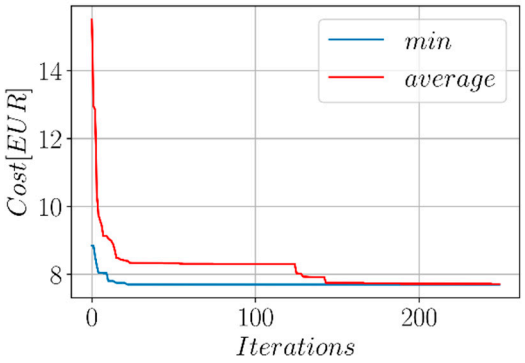

(**c**) $N_{u,min}$ = 3000 kN

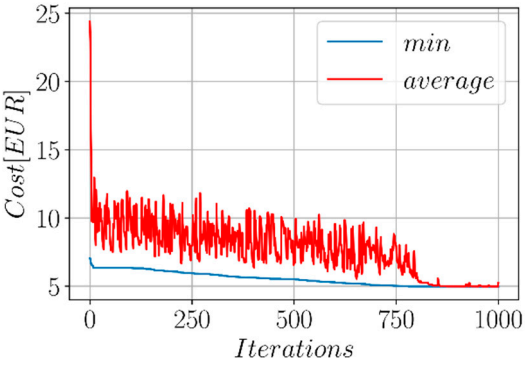

(**d**) $N_{u,\ min}$ = 2000 kN

Figure 13. Variation of cost for f'_c = 60 MPa, (Turkey).

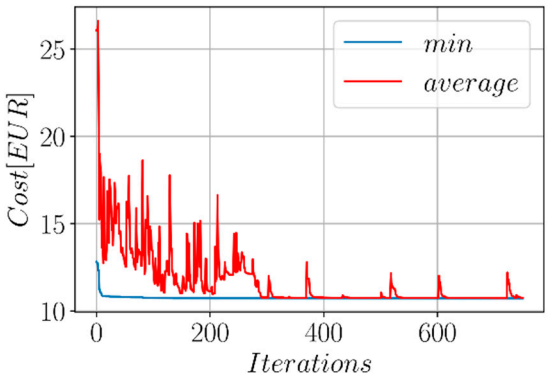

(**a**) $N_{u,\ min}$ = 6000 kN

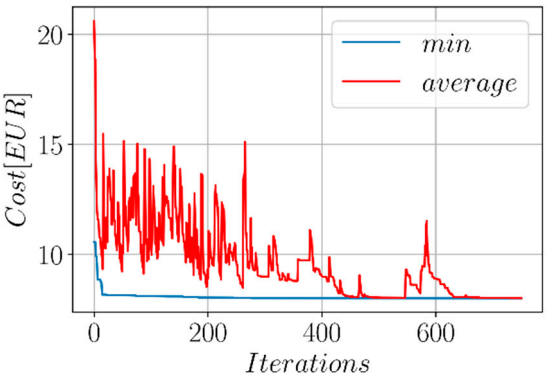

(**b**) $N_{u,\ min}$ = 4000 kN

Figure 14. *Cont.*

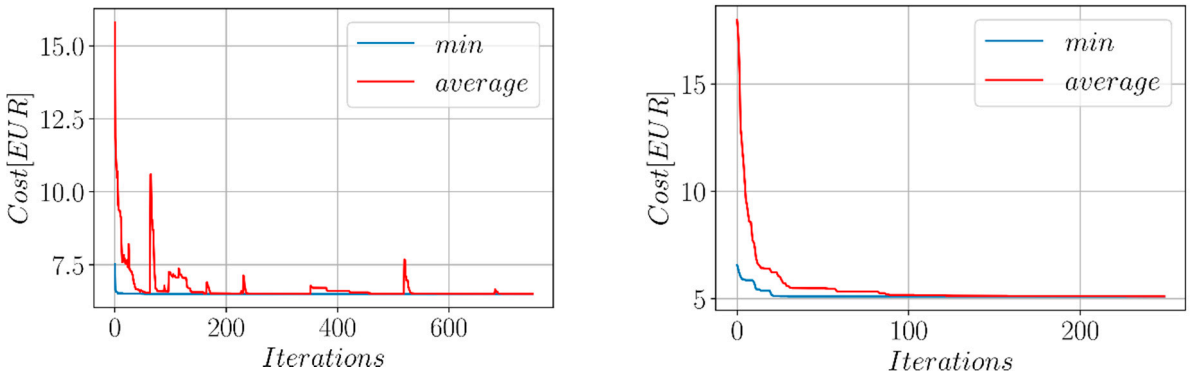

(**c**) $N_{u,\ min}$ = 3000 kN (**d**) $N_{u,\ min}$ = 2000 kN

Figure 14. Variation of cost for f_c' = 25 MPa, (Turkey).

Table 6. Optimum configurations based on cost (Turkey).

f_c' [MPa]	D [mm]	t [mm]	D/t	$N_{u,min}$ [kN]	Cost [EUR]
60	272.18	3.04	89.53	6000	11.49
60	244.47	2.96	82.59	5000	9.9
60	212.37	2.96	71.75	4000	8.38
60	161.20	3.89	41.44	3000	7.70
60	134.91	2.96	45.58	2000	4.97
60	126.37	2.97	42.55	1000	4.44
40	268.64	3.20	83.95	6000	11.58
40	244.47	2.96	82.59	5000	9.71
40	212.37	2.96	71.75	4000	8.24
40	176.47	2.96	59.62	3000	6.66
40	134.91	2.96	45.58	2000	4.91
40	125.78	3.22	39.06	1000	4.40
25	273.79	2.96	92.50	6000	10.72
25	244.47	2.96	82.59	5000	9.41
25	212.37	2.96	71.75	4000	8.01
25	176.47	2.96	59.62	3000	6.50
25	129.60	3.31	39.15	2000	5.10
25	122.89	3.11	39.52	1000	4.32

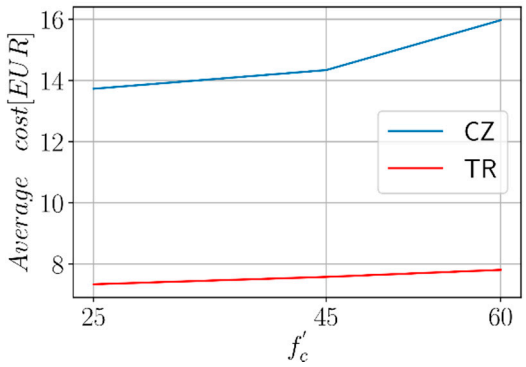

Figure 15. Average cost for each concrete class.

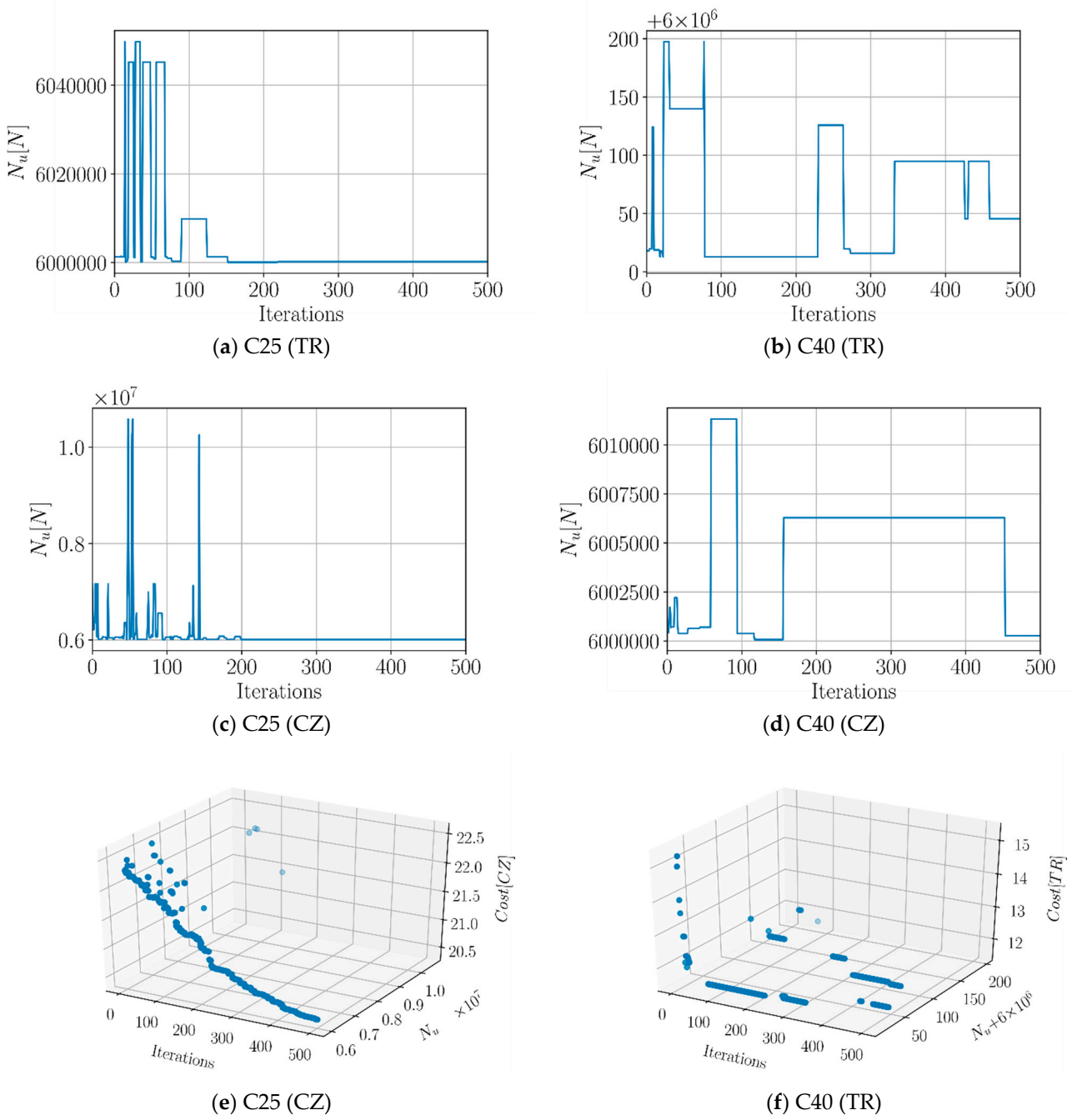

(**a**) C25 (TR) (**b**) C40 (TR)

(**c**) C25 (CZ) (**d**) C40 (CZ)

(**e**) C25 (CZ) (**f**) C40 (TR)

Figure 16. Variation of N_u throughout the cost optimization.

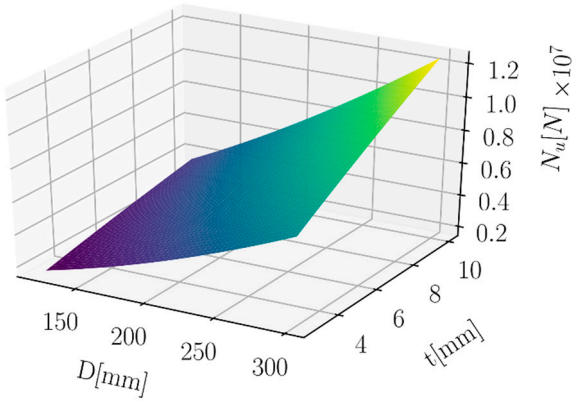

Figure 17. Variation of N_u with respect to geometry.

6. Conclusions

In this study, the application of the social spider algorithm to the cross-sectional optimization of CFST columns has been demonstrated. The ultimate axial load-carrying capacity of the columns was introduced as a design constraint such that only the designs leading to a certain level of load-carrying capacity are considered. Among the various equations in the literature that predict the axial load-carrying capacity of CFST columns, the set of equations developed by Wang et al. [7] was adopted for the calculation of N_u. This set of equations was considered to be the most suitable because of the wide ranges of parameters to which the equations are applicable. The design optimization was carried out for CFST stub columns with unit height, considering the CO_2 emission and cost in two different jurisdictions as the quantities to be minimized. The key outcomes of this study are listed as follows:

- The results of the optimization showed that, on average, using concrete with lower compressive strength is favorable in terms of both CO_2 emissions and cost.
- In general, having a smaller wall thickness for the steel casing has a favorable effect on both the CO_2 emissions and the cost since the optimum wall thickness is near the lower bound for this variable at most load levels.
- In the majority of the investigated cases, a decrease in the outer diameter and the D/t ratio was also associated with a decrease in cost and CO_2 emissions.
- Designs that lead to lower carbon emissions also tend to have a lower cost.

Further research in this field can be carried out on concrete-filled columns with rectangular cross-sections. Additionally, structures with uniform material properties such as steel columns could be optimized with respect to their load-carrying capacities, cross-sectional dimensions, or slenderness properties. Furthermore, the number of variables affecting the load-carrying capacity as well as the number of constraints could be increased. Future studies can also include the unit prices of additional jurisdictions in the optimization. The scope of the optimization could also be extended from stub columns to include slender columns as well. Moreover, a sensitivity analysis could be carried out encompassing the variables affecting the structural performance.

Author Contributions: C.C. and G.B. generated the analysis codes. The text of the paper was formed by C.C., K.I., G.B. and M.B. The figures were prepared by C.C., K.I., G.B. and M.B. supervised the research direction. All authors have read and agreed to the published version of the manuscript.

Funding: This research received no external funding.

Conflicts of Interest: The authors declare no conflict of interest.

References

1. Wei, J.; Luo, X.; Lai, Z.; Varma, A.H. Experimental Behavior and Design of High-Strength Circular Concrete-Filled Steel Tube Short Columns. *J. Struct. Eng.* **2019**, *146*, 04019184. [CrossRef]
2. Nguyen, T.T.; Thai, H.T.; Ngo, T.; Uy, B.; Li, D. Behaviour and design of high strength CFST columns with slender sections. *J. Constr. Steel Res.* **2021**, *182*, 106645. [CrossRef]
3. Duong, H.T.; Phan, H.C.; Le, T.T.; Bui, N.D. Optimization design of rectangular concrete-filled steel tube short columns with Balancing Composite Motion Optimization and data-driven model. *Structures* **2020**, *28*, 757–765. [CrossRef]
4. Shieh, S.S.; Chang, C.C.; Jong, J.H. Structural design of composite super-columns for the Taipei 101 Tower. In Proceedings of the International Workshop on Steel and Concrete Composite Constructions, Sydney, Australia, 22–25 June 2003; pp. 25–33.
5. Han, L. Tests on stub columns of concrete-filled RHS sections. *J. Constr. Steel Res.* **2002**, *58*, 353–372. [CrossRef]
6. Han, L.; Yao, G.; Zhao, X. Tests and calculations for hollow structural steel (HSS) stub columns filled with self-consolidating concrete (SCC). *J. Constr. Steel Res.* **2005**, *61*, 1241–1269. [CrossRef]
7. Schneider, S. Axially Loaded Concrete-Filled Steel Tubes. *J. Struct. Eng.* **1998**, *124*, 1125–1138. [CrossRef]
8. Sakino, K.; Tomii, M.; Watanabe, K. Sustaining load capacity of plain concrete stub columns by circular steel tubes. In Proceedings of the International Speciality Conference on Concrete-Filled Steel Tubular Structure, Harbin, China, 12–15 August 1985; pp. 112–118.
9. Huang, F.; Yu, X.; Chen, B. The structural performance of axially loaded CFST columns under various loading conditions. *Steel Compos. Struct.* **2012**, *13*, 451–471. [CrossRef]
10. Yang, Y.F.; Ma, G.L. Experimental behaviour of recycled aggregate concrete filled stainless steel tube stub columns and beams. *Thin Walled Struct.* **2013**, *66*, 62–75. [CrossRef]
11. Uenaka, K.; Kitoh, H.; Sonoda, K. Concrete Filled Double Skin Circular Stub Columns Under Compression. *Thin-Walled Struct.* **2010**, *48*, 19–24. [CrossRef]
12. Perea, T.; Leon, R.T.; Hajjar, J.F.; Denavit, M.D. Full-Scale Tests of Slender Concrete-Filled Tubes: Axial Behavior. *J. Struct. Eng.* **2013**, *139*, 1249–1262. [CrossRef]
13. American Institute of Steel Construction (AISC). *Specification for Structural Steel Buildings*; AISC 360-16; American Institute of Steel Construction: Chicago, IL, USA, 2016.
14. European Committee for Standardization (CEN). *Design of Composite Steel and Concrete Structures—Part 1-1: General Rules and Rules for Buildings*; EN 1994-1-1 Eurocode 4; European Committee for Standardization: Brussels, Belgium, 2004.
15. Canadian Standards Association. *Design of Steel Structures—CSA S16*, 9th ed.; Canadian Standards Association: Mississauga, ON, Canada, 2019; ISBN 978-1-4883-1548-0.
16. Standards Australia. *AS 5100.1 2017: Bridge Design, Part 1: Scope and General Principles*; Standards Australia: Sydney, Australia, 2017.
17. Liu, D.; Gho, W.M. Axial load behaviour of high-strength rectangular concrete-filled steel tubular stub columns. *Thin Walled Struct.* **2005**, *43*, 1131–1142. [CrossRef]
18. Thai, H.T.; Uy, B.; Khan, M.; Tao, Z.; Mashiri, F. Numerical modelling of concrete-filled steel box columns incorporating high strength materials. *J. Constr. Steel Res.* **2014**, *102*, 256–265. [CrossRef]
19. Khan, M.; Uy, B.; Tao, Z.; Mashiri, F. Concentrically loaded slender square hollow and composite columns incorporating high strength properties. *Eng. Struct.* **2016**, *131*, 69–89. [CrossRef]
20. Khan, M.; Uy, B.; Tao, Z.; Mashiri, F. Behaviour and design of short high-strength steel welded box and concrete-filled tube (CFT) sections. *Eng. Struct.* **2017**, *147*, 458–472. [CrossRef]
21. Saadoon, A.S.; Nasser, K.Z. Mohamed IQ. A neural network model to predict ultimate strength of rectangular concrete filled steel tube beam-columns. *Eng. Technol. J.* **2012**, *30*, 3328–3340.
22. Saadoon, A.S.; Nasser, K.Z. Use of neural networks to predict ultimate strength of circular concrete filled steel tube beam-columns. *Univ. Thi-Qar J. Eng. Sci.* **2013**, *4*, 48–62.
23. Ahmadi, M.; Naderpour, H.; Kheyroddin, A. ANN model for predicting the compressive strength of circular steel-confined concrete. *Int. J. Civ. Eng.* **2017**, *15*, 213–221. [CrossRef]
24. Le, T.-T. Surrogate neural network model for prediction of load-bearing capacity of CFSS members considering loading eccentricity. *Appl. Sci.* **2020**, *10*, 3452. [CrossRef]
25. Fantilli, A.P.; Mancinelli, O.; Chiaia, B. The carbon footprint of normal and high-strength concrete used in low-rise and high-rise buildings. *Case Stud. Constr. Mater.* **2019**, e00296. [CrossRef]
26. Youn, M.H.; Park, K.T.; Lee, Y.H.; Kang, S.-P.; Lee, S.M.; Kim, S.S.; Kim, Y.E.; Na Ko, Y.; Jeong, S.K.; Lee, W. Carbon dioxide sequestration process for the cement industry. *J. CO_2 Util.* **2019**, *34*, 325–334. [CrossRef]
27. Faridmehr, I.; Nehdi, M.L.; Nikoo, M.; Huseien, G.F.; Ozbakkaloglu, T. Life Cycle Assessment of Alkali-Activated Materials Incorporating Industrial Byproducts. *Materials* **2021**, *14*, 2401. [CrossRef] [PubMed]
28. Yeo, D.; Potra, F.A. Sustainable Design of Reinforced Concrete Structures through CO_2 Emission Optimization. *J. Struct. Eng.* **2015**, *141*, B4014002. [CrossRef]
29. Kayabekir, A.E.; Arama, Z.A.; Bekdaş, G.; Nigdeli, S.M.; Geem, Z.W. Eco-friendly design of reinforced concrete retaining walls: Multi-objective optimization with harmony search applications. *Sustainability* **2020**, *12*, 6087. [CrossRef]

30. Paik, I.; Na, S. Comparison of Carbon Dioxide Emissions of the Ordinary Reinforced Concrete Slab and the Voided Slab System During the Construction Phase: A Case Study of a Residential Building in South Korea. *Sustainability* **2019**, *11*, 3571. [CrossRef]
31. Ženíšek, M.; Pešta, J.; Tipka, M.; Kočí, V.; Hájek, P. Optimization of RC Structures in Terms of Cost and Environmental Impact—Case Study. *Sustainability* **2020**, *12*, 8532. [CrossRef]
32. Turkish Ministry of Environment and Urbanisation. *Construction Unit Costs*; Directorate of Higher Technical Board: Ankara, Turkey, 2020.
33. American Concrete Institute (ACI). *Building Code Requirements for Structural Concrete and Commentary*; ACI 318-11; American Concrete Institute: Farmington Hills, MI, USA, 2011.
34. Tao, Z.; Wang, Z.B.; Yu, Q. Finite element modelling of concrete-filled steel stub columns under axial compression. *J. Constr. Steel Res.* **2013**, *89*, 121–131. [CrossRef]
35. Uy, B.; Tao, Z.; Han, L.H. Behaviour of short and slender concrete-filled stainless steel tubular columns. *J. Constr. Steel Res.* **2011**, *67*, 360–378. [CrossRef]
36. Wang, Z.-B.; Tao, Z.; Han, L.-H.; Uy, B.; Lam, D.; Kang, W.-H. Strength, stiffness and ductility of concrete-filled steel columns under axial compression. *Eng. Struct.* **2017**, *135*, 209–221. [CrossRef]
37. Sakino, K.; Nakahara, H.; Morino, S.; Nishiyama, I. Behavior of Centrally Loaded Concrete-Filled Steel-Tube Short Columns. *J. Struct. Eng.* **2004**, *130*, 180–188. [CrossRef]
38. Lai, Z. Experimental Database, Analysis and Design of Noncompact and Slender Concrete-Filled Steel Tube (CFT) Members. Ph.D. Thesis, Purdue University, West Lafayette, IN, USA, 2014.
39. Islam, M. Experimental investigation on concentrically loaded square concrete-filled steel tubular columns. Master's Science Thesis, Bangladesh University of Engineering and Technology, Dhaka, Bangladesh, 2019.
40. Geem, Z.W.; Kim, J.H.; Loganathan, G.V. A New Heuristic Optimization Algorithm: Harmony Search. *Simulation* **2001**, *76*, 60–68. [CrossRef]
41. Bekdaş, G. Harmony Search Algorithm Approach for Optimum Design of Post-Tensioned Axially Symmetric Cylindrical Reinforced Concrete Walls. *J. Optim. Theory Appl.* **2014**, *164*, 342–358. [CrossRef]
42. Kennedy, J.; Eberhart, R. Particle swarm optimization. In Proceedings of the 1995 IEEE International Conference on Neural Networks, Perth, Australia, 27 November–1 December 1995; Volume 4, pp. 1942–1948.
43. Karaboga, D. *An İdea Based on Honey Bee Swarm for Numerical Optimization*; Technical Report-TR06; Engineering Faculty, Computer Engineering Department, Erciyes University: Kayseri, Turkey, 2005.
44. Karaboga, D.; Akay, B. A comparative study of artificial bee colony algorithm. *Appl. Math. Comput.* **2009**, *214*, 108–132. [CrossRef]
45. Abachizadeh, M.; Tahani, M. An ant colony optimization approach to multi-objective optimal design of symmetric hybrid laminates for maximum fundamental frequency and minimum cost. *Struct. Multidiscip. Optim.* **2008**, *37*, 367–376. [CrossRef]
46. Kayabekir, A.E. Effects of Constant Parameters on Optimum Design of Axially Symmetric Cylindrical Reinforced Concrete Walls. *Struct. Des. Tall Spec. Build.* **2021**, *30*, e1838. [CrossRef]
47. Alrashidi, M.; Rahman, S.; Pipattanasomporn, M. Metaheuristic optimization algorithms to estimate statistical distribution parameters for characterizing wind speeds. *Renew. Energy* **2020**, *149*, 664–681. [CrossRef]
48. Cuevas, E.; Cienfuegos, M.; Zaldívar, D.; Pérez-Cisneros, M. A swarm optimization algorithm inspired in the behavior of the social-spider. *Expert Syst. Appl.* **2013**, *40*, 6374–6384. [CrossRef]
49. Maxence, S. Social organization of the colonial spider Leucauge sp. in the Neotropics: Vertical stratification within colonies. *J. Arachnol.* **2010**, *38*, 446–451.